Crystal Structure of Nitric Oxide Synthase Bound to Nitro Indazole Reveals a Novel Inactivation Mechanism†

C. S. Raman,*,‡,§ Huiying Li,‡,§ Pavel Martásek,||,⊥ Garry Southan,# Bettie Sue S. Masters,|| and Thomas L. Poulos*,‡

Departments of Molecular Biology & Biochemistry and Physiology & Biophysics and the Program in Macromolecular Structure, University of California, Irvine, California 92697, Department of Biochemistry, University of Texas Health Science Center, San Antonio, Texas 78229, Department of Pediatrics, First Medical Faculty, Charles University, Prague, Czech Republic, and Inotek Corp., Beverly, Massachusetts 01915

Received May 10, 2001; Revised Manuscript Received August 27, 2001

ABSTRACT: Nitric oxide is generated under normal and pathophysiological conditions by three distinct isoforms of nitric oxide synthase (NOS). A small-molecule inhibitor of NOS (3-Br-7-nitroindazole, 7-NIBr) is profoundly neuroprotective in mouse models of stroke and Parkinson's disease. We report the crystal structure of the catalytic heme domain of endothelial NOS complexed with 7-NIBr at 1.65 Å resolution. Critical to the binding of 7-NIBr at the substrate site is the adoption by eNOS of an altered conformation, in which a key glutamate residue swings out toward one of the heme propionate groups. Perturbation of the heme propionate ensues and eliminates the cofactor tetrahydrobiopterin−heme interaction. We also present three crystal structures that reveal how alterations at the substrate site facilitate 7-NIBr and structurally dissimilar ligands to occupy the cofactor site.

Nitric oxide (NO)[1] is a key signaling molecule in human physiology (*1*−*3*) with soluble guanylyl cyclase (sGC) serving as the hemoprotein receptor for NO (*4*). Upon NO binding, sGC is activated and converts GTP to cGMP, thereby facilitating signal transduction (*5*). A family of three enzymes, collectively known as nitric oxide synthases (NOS) (*6*), catalyzes the oxidation of a terminal guanidinium nitrogen of the amino acid L-arginine resulting in NO biosynthesis (*7*, *8*). Two of these isoforms (endothelial and neuronal NOS) are constitutive in that they support transient production of NO suitable for cellular signaling. NO generated by the endothelial NOS (eNOS) is involved in the regulation of blood pressure, organ blood flow distribution, and inhibition of platelet aggregation. NO derived from the neuronal NOS (nNOS) functions as a neurotransmitter in the brain. Excessive NO generation in the central nervous system, however, leads to neuropathology. For example, nNOS mutant mice deficient in neuronally derived NO exhibit a remarkably increased resistance to stroke (*9*). The nonconstitutive isoform of NOS (iNOS) is transcriptionally induced by pro-inflammatory agents such as endotoxin (bacterial lipopolysaccharide), interleukin-12, and other cytokines in a variety of cell types. Overproduction of NO by iNOS has been implicated in a number of pathological conditions including septic shock (*10*).

NOS is an important drug target (*11*), and isoform-selective inhibitors are needed to block the uncontrolled production of NO in disease states (*12*). It is critical that these inhibitors not affect eNOS as it would severely perturb blood pressure homeostasis. Identification of NOS inhibitors have focused heavily on L-Arg-like compounds that target the substrate-binding site on the catalytic heme domain. Furthermore, the design of potent isoform-specific inhibitors has been made difficult by the strong structural similarity (*13*−*15*) exhibited by the L-Arg binding site on all three NOS isoforms. Nevertheless, as evidenced by the development of COX-2 inhibitors (*16*−*18*), isoform-selective inhibitor design holds great promise for NOS.

We hypothesized that compounds with little or no structural similarity to the substrate L-Arg could exhibit unique modes of binding to NOS. In addition, we conjectured that conformational changes induced by these compounds might provide key insights that could not otherwise be obtained from those inhibitors that bound without perturbing the binding site. To this end, we have determined the crystal structure of 3-Br-7-nitroindazole (7-NIBr, Figure 1) complexed with the catalytic heme domain of eNOS. Both 7-nitroindazole (7-NI) (*19*−*21*) and 7-NIBr (*22*) are potent inhibitors of all three NOS isoforms in vitro. Biochemical studies have shown that these compounds not only compete with L-Arg but also for the cofactor tetrahydrobiopterin (H_4B)-binding site (*23*−*25*). These inhibitors, however, exhibit a high level of specificity for nNOS in vivo and fail

† This work was supported by NIH Grants GM 57353 (T.L.P.) and GM52419 (B.S.S.M.) and Robert A. Welch Grant AQ-1192 (B.S.S.M.). The contribution of P.M. was partially supported by the Czech Grant Agency No. GACR 306/99/0054.

* To whom correspondence should be addressed. (C.S.R) E-mail: c.s.raman@uth.tmc.edu. Phone: (713) 500-6285. Fax: (713) 500-0651. (T.L.P.) E-mail: poulos@uci.edu. Phone: (949) 824-7020. Fax: (949) 824-3280.

‡ Departments of Molecular Biology & Biochemistry and Physiology & Biophysics.

§ These authors contributed equally to this work.

|| Department of Biochemistry.

⊥ Department of Pediatrics.

Inotek Corp.

[1] Abbreviations: NOS, nitric oxide synthase; 7-NI, 7-nitroindazole; 7-NIBr, 3-bromo-7-nitroindazole; L-NNA, N^{ω}-nitro-L-Arg; NICA; 7-nitroindazole-2-carboxamidine; CPHG, 4-chlorophenyl hydroxyguanidine; H_4B, tetrahydrobiopterin.

10.1021/bi010957u CCC: $20.00
Published on Web 10/20/2001

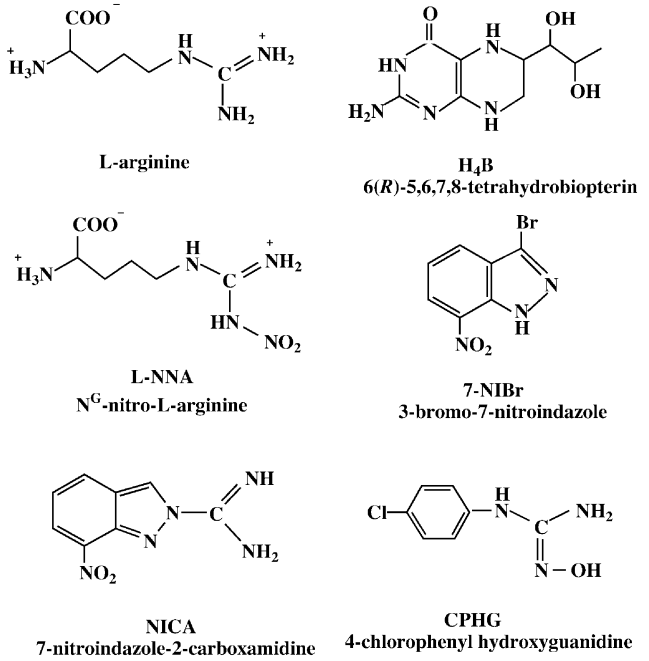

FIGURE 1: Structural formulas of substrate, cofactor, and the ligands used in this crystallographic study.

to produce discernible changes in systemic blood pressure (*20*, *26*). Although the exact mechanism for the specificity of these inhibitors to nNOS in vivo is poorly understood, it is thought that differences in uptake pathways of different cell types may play a role. More importantly, 7-NI and 7-NIBr are extremely neuroprotective in animal models of stroke (*27*) and Parkinson's disease (*28*, *29*). Therefore, understanding the molecular basis of 7-NIBr recognition by NOS will aid in the development of new isoform-selective inhibitors that can be used in the treatment of neurodegenerative disorders involving NO-mediated neurotoxicity.

A fundamental insight arising from our work on 7-NIBr complexed eNOS is a structural demonstration of the cooperativity between the substrate- and cofactor-binding sites in NOS and the dynamics of the key active-site residue Glu-363. These results will have important ramifications for the design of isoform-selective NOS inhibitors targeted to either the substrate, cofactor, or both binding sites.

EXPERIMENTAL PROCEDURES

L-NNA and 7-NIBr were purchased from Alexis and Calbiochem, respectively. NICA (*30*) and CPHG (*31*) were synthesized according to the published procedures.

Bovine endothelial NOS heme domain protein sample was generated by trypsinolysis from the holo-eNOS expressed in *Escherichia coli* (*15*, *32*). For the pterin-free protein preparations, H_4B was omitted in all buffers used during purification. The eNOS−inhibitor complex crystals were grown at 280 K using the sitting drop vapor diffusion method developed for the substrate complex, so that the only difference here is to replace L-Arg with millimolar amounts of inhibitors in the crystallization cocktail (*15*). H_4B was not added to either the protein or mother liquor prior to or after crystallization.

Cryogenic (100 K) X-ray diffraction data were collected at various synchrotron facilities: Stanford Synchrotron Radiation Laboratory (SSRL) BL7-1 or BL9-1 with a MarResearch Mar345 imaging plate, the Cornell High Energy Synchrotron Source (CHESS) Beamline F2 with an ADSC Quantum 1 CCD detector, and the Advanced Light Source (ALS) BL5.0.2 with an ADSC Quantum 4 CCD detector. The raw data frames were integrated and scaled with the HKL Suite (*33*). To locate the bound ligands, difference Fourier electron density maps were calculated with CNS (*34*). Once the model of ligands was built into the structures using TOM/FRODO (*35*), further structure refinements were carried out with CNS or SHELXL (*36*). Data collection and refinement statistics are summarized in Table 1. Omit $2F_o - F_c$ electron density maps of three complex structures shown in Figure 2 were generated by running simulated annealing protocol in CNS at initial temperature of 1000 K with the ligand of interest omitted during the calculation.

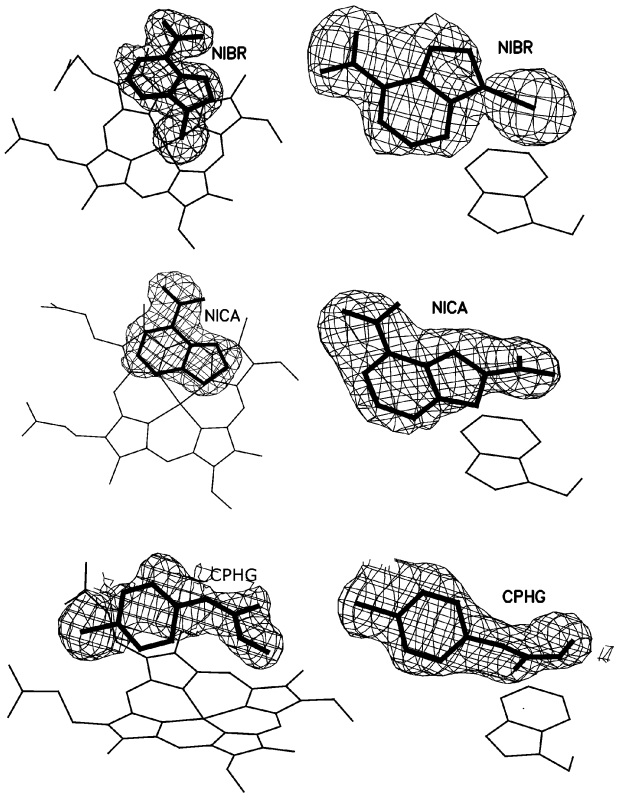

FIGURE 2: Omit $2F_o - F_c$ electron density maps, contoured at 1σ, of 7-NIBr, NICA and CPHG at both the substrate and cofactor binding sites with heme group and Trp-449 shown in the background, respectively.

RESULTS AND DISCUSSION

Molecular Recognition of 7-NIBr at the Substrate Binding Site. The active-site structure of eNOS is shown in Figure 3. The substrate, L-Arg, is positioned over the heme where H-bonds with the conserved Glu-363 help to orient the substrate for regioselective hydroxylation by, presumably, an Fe-linked O atom. The essential cofactor, H_4B, is bound at the intersubunit interface. Note that H_4B and the α-amino group of L-Arg both H-bond with the same heme propionate. Presumably, 7-NIBr displaces L-Arg from the active site despite the fact that 7-NIBr bears no structural similarity to L-Arg. To understand how 7-NIBr binds to NOS, we solved the crystal structure of 7-NIBr bound to the catalytic heme domain of eNOS at 1.65 Å resolution. Strong electron density

Table 1: Data Collection and Refinement Statistics

data set[a]	NIBR1	NIBR2	NICA	CPHG	NNA1	NNA2
PDB code	1D0C	1D0O	1FOJ	2DM6	1ED5	8NSE
cell dimensions (Å)						
(space group: $P2_12_12_1$)						
a	57.44	57.59	58.38	58.20	58.82	58.31
b	105.98	106.06	106.49	106.56	106.42	105.78
c	155.79	155.78	155.70	156.67	156.16	156.61
data resolution (Å)	1.65	1.95	2.10	1.95	1.80	2.25
total observations	398 353	231 841	141 597	174 140	314 057	153 298
unique reflections	114 549	73 044	54 878	63 487	87 722	44 385
R_{sym}[b]	0.048	0.050	0.058	0.068	0.061	0.052
	(0.586)[c]	(0.612)	(0.761)	(0.779)	(0.639)	(0.216)
$\langle I/\sigma \rangle$	11.5	8.8	8.4	6.2	9.2	16.4
	(2.1)[c]	(2.0)	(1.5)	(1.2)	(1.7)	(2.5)
completeness	0.984	0.957	0.952	0.896	0.971	0.963
	(0.991)[c]	(0.935)	(0.965)	(0.897)	(0.996)	(0.691)
reflection used in refinement	112 609	58 970	50 855	58 892	77 286	39 054
R-factor[d]	0.213	0.200	0.227	0.220	0.220	0.227
R-free[e]	0.259	0.247	0.259	0.255	0.254	0.276
no. of protein atoms	6593	6593	6593	6593	6593	6593
no. of heteroatoms	179	173	163	157	155	157
no. of waters	655	426	372	516	633	206
RMS deviation						
bond length (Å)	0.009	0.008	0.007	0.007	0.008	0.007
bond angle (deg)	0.023 Å	1.4	1.4	1.3	1.4	1.4

[a] NIBR1 and NIBR2, 3-bromo-7-nitroindazole with the H_4B-free and -bound protein, respectively; NICA, 7-nitroindazole-2-carboxamidine; CPHG, *N*-(4-chlorophenyl)-*N*′-hydroxyguanidine; NNA1 and NNA2, N^{ω}-nitro-L-arginine with the H_4B-free and -bound protein, respectively. [b] $R_{sym} = \sum|I - \langle I \rangle|/\sum I$, where *I* is the observed intensity and $\langle I \rangle$ the averaged intensity of multiple symmetry related observations of the reflection. [c] The values in parentheses were obtained in the outermost resolution shell. [d] *R*-factor $= \sum||F_o| - F_c||/\sum|F_o|$, F_o and F_c are the observed and calculated structure factors, respectively. [e] *R*-free was calculated with the 5% of reflections set aside randomly throughout the refinement. The same set of reflections were chosen for every data set.

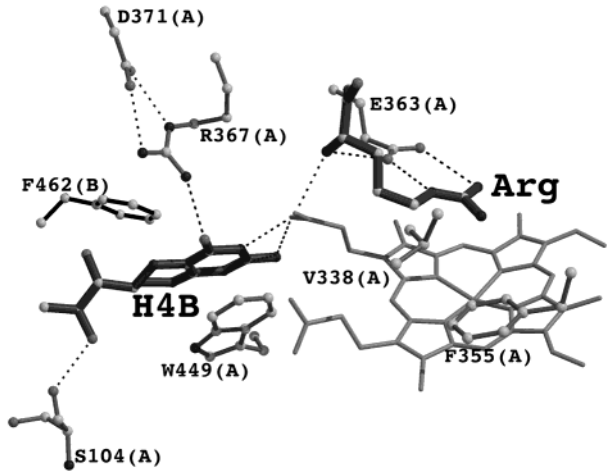

FIGURE 3: A molecular model of the eNOS active and H_4B binding sites. Note that L-Arg and H_4B both H-bond with the same heme propionate.

for 7-NIBr occupies the site where L-Arg is normally bound (Figure 2). The orientation of the inhibitor is unambiguous due to the bulky density of the bromine atom used as a guide in positioning the inhibitor into its electron density. When compared with the contoured surface of the substrate or inhibitors that resemble L-Arg (*15*), 7-NIBr is relatively planar and stacks parallel within van der Waals contact distance to the heme plane (Figure 4A). The pyrazole nitrogen atoms do not coordinate the heme iron. An oxygen atom from the nitro group of 7-NIBr establishes a close nonbonded contact with the methyl group of pyrrole A. C4 and C9 of the inhibitor are ~4.0 Å away from the heme iron. N1 of 7-NIBr assumes a position similar to one of the terminal guanidine nitrogen atoms of the substrate and, like the substrate, donates an H-bond to the carbonyl O of Trp-358. 7-NIBr forms a second H-bond with the protein that is between the nitro group and peptide NH of Met-360. In addition to these two H-bonds, many (31) nonbonded contacts exist between the inhibitor and the protein with bromine participating in roughly one-fourth (7) of these contacts.

A striking difference between the substrate (*15*) and 7-NIBr bound crystal structures is the position of the Glu-363 side chain (Figure 4A). Glu-363 was known to be critical for NOS function (*37*, *38*) prior to the crystal structures which show that Glu-363 forms specific H-bonding interactions with L-Arg. In the 7-NIBr bound structure Glu-363 assumes a different rotameric state (χ_1 of 165°) than that observed in the L-Arg bound form (χ_1 of −65°). This rotameric state places the Glu-363 side chain in the proximity of one of the heme propionates, requiring the heme propionate also to move. The nitro group of 7-NIBr nicely fills the void left behind by the Glu-363 side chain. For example, the H-bond between Met-360 NH and Glu-363 OE1 in the L-Arg bound structure is replaced by one involving the nitro group (vide supra).

7-NIBr, being an aromatic heterocycle, albeit π-deficient at carbon atoms due to the increase in number of ring N atoms, probably derives some of its binding energy from the $\pi-\pi$ stacking interactions with the heme and many nonbonded contacts it entertains with the protein. Nevertheless, the driving force behind the molecular recognition of 7-NIBr at the substrate-binding site cannot solely arise from stacking interactions since indazole, per se, is not an inhibitor of NOS (*39*). This leaves the nitro group as the most distinguishing feature that accounts for the potency of 7-NIBr and 7-NI with K_D values in the range of 100 nM (*24*). In

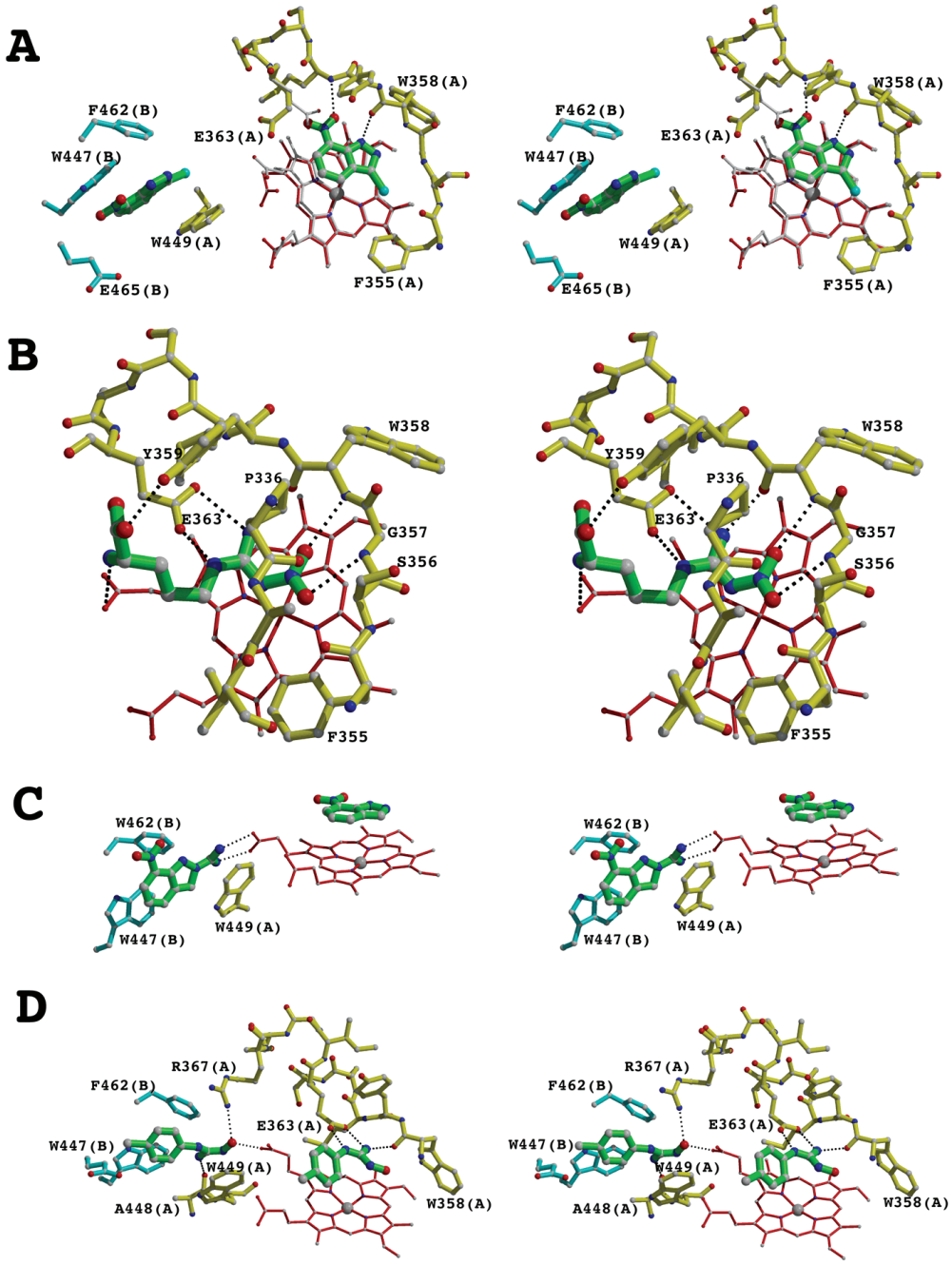

FIGURE 4: Stereomodels of the various complexes used in this study. The inhibitors are green, residues in subunit A yellow, and residues in subunit B cyan. Dashed lines indicate H-bonding interactions. The color schemes used for elements are carbon, light gray; nitrogen, blue; oxygen, red. (A) The 7-NIBr complex showing the inhibitor bound at both the L-Arg and H_4B binding sites. The heme and position of Glu-363 in the eNOS-L-Arg complex are shown as white models to highlight the change in the orientation of Glu-363 and one heme propionate. (B) The L-NNA complex. There is no difference in the binding of L-NNA in the pterin-free or -bound structures so only the pterin-bound structure (pterin site not included) is shown. (C) The NICA complex. Note that NICA at the active site no longer has the carboxamidine group probably due to slight contamination with 7-NI, a starting material in the synthesis of NICA. (D) The CPHG complex with the inhibitor bound at both the substrate and H_4B binding sites.

addition to providing an extra H-bonding interaction with the protein, the electron-withdrawing properties of the nitro group imparts a partial positive charge on the indazole aromatic ring compared to unsubstituted indazole. A DELPHI (*40*) electrostatic calculation shows that 7-NIBr is situated in a large electronegative potential owing primarily to Glu-363, despite its movement away from the inhibitor, and the heme propionate. Thus, the 7-NIBr ring mimics the L-Arg guanidinium in both electrostatic stabilization and π-stacking with the heme ring. It thus appears that the two unique features of 7-NIBr that can help explain its potency as a NOS inhibitor compared to other indazoles is the nitro-peptide H-bond and electrostatic stabilization of the partial positive charge on the indazole ring which provides greater electrostatic complementarity at the active site than unsubstituted indazoles.

Structural Determinants of 7-NIBr Binding to the Cofactor Site. A surprising finding in the 7-NIBr-complexed crystal structure is that 7-NIBr not only interacts with the substrate-binding site but also binds to the cofactor site (Figure 4A). Pterin-free eNOS was used in the cocrystallization experiments since we have routinely (*15*) used this form of the

protein in structure determination. The electron density of the inhibitor is clearly discernible (Figure 2), and the data quality in conjunction with the strong density corresponding to the Br atom removes any ambiguities on the orientation of the inhibitor. There are no changes in the position of main-chain and side-chain atoms of the H_4B site. The nearly perfect stacking interactions observed with 7-NIBr bound at the substrate-binding site are not observed at the cofactor-binding site despite the abundance of aromatic side chains. There is a partial stacking interaction between 7-NIBr and Trp-447 from the second subunit (Figure 4A). In addition, there are no H-bonds between the inhibitor and protein in the cofactor binding site. Nonbonded contacts, nearly twice as many as those in the substrate site, are fully responsible for the recognition of 7-NIBr at the cofactor site. Roughly one-third (22) of the nonbonded contacts between the inhibitor and protein are made with one subunit and includes six of seven interactions made by the Br atom. Five of these six interactions are made with Trp-449 since Br sits on top of the indole ring. The remaining two-thirds (40) of the nonbonded contacts are made with the second subunit. A preponderance of inhibitor contacts with the latter involve the aromatic main- and side-chain (Trp-76, Trp-447, and Phe-462) atoms. One striking observation is the close proximity of Glu-465, from the second subunit, to the nitro group of 7-NIBr, which is reminiscent of Glu-363 and its interactions with the inhibitor at the substrate-binding site. Nearly all atoms of Glu-465, with the exception of CD, OE1, and OE2, are within 4.0 Å of one of the nitro oxygen atoms, with CG and backbone N exhibiting the closest distance of separation. An important difference, however, is that the side-chain carboxylate of Glu-465, unlike Glu-363 at the L-Arg binding site, is anchored via three H-bonded contacts to main-chain and side-chain atoms.

7-NIBr Binding to the Substrate Site Perturbs H_4B Interaction With eNOS. To test whether 7-NIBr binding at the substrate site directly impedes cofactor binding, we cocrystallized 7-NIBr with eNOS already complexed to H_4B. For this purpose, we utilized eNOS heme domain protein that was purified in the presence of exogenously added H_4B to ensure that the cofactor sites in both subunits would be fully occupied. The crystal structure of the 7-NIBr complex of eNOS thus obtained reveals that the cofactor is no longer bound and 7-NIBr has instead taken its place (Figure 4A). This structure is indistinguishable from one in which 7-NIBr was cocrystallized with the pterin-free protein. Regardless of whether the starting material was H_4B-free or H_4B-bound, cocrystallization in the presence of 7-NIBr resulted in two molecules of the inhibitor bound per subunit—one at the substrate binding site and the other occupying the pterin-binding site. A structural model for how alterations at one binding site affects another site can therefore be proposed. To accommodate 7-NIBr in the active site, Glu-363 must adopt a new rotomeic state near one of the heme propionate groups. As a result, the heme propionate group also must move. This same propionate H-bonds with both H_4B and L-Arg in catalytically competent NOS (*13*−*15*), thereby mediating the cross-talk between the substrate and H_4B binding sites. Hence, an alteration in the conformation of this key propionate will alter its ability to effectively H-bond to both H_4B and the substrate. The 1.65 Å resolution structure of 7-NIBr-bound eNOS heme domain reveals three distinct conformations of the heme propionate that would otherwise be interacting with the cofactor and substrate. In one subunit, we observe two alternate conformations characterized by Glu-363 OE1—heme propionate O2A, a distance of 2.6 and 3.8 Å, respectively. In the second subunit, the distance of separation between these two atoms is slightly larger (4.2 Å). In the alternative conformation, the carboxylate of one propionate is bent over, pointing to the other propionate group. These results provide strong evidence for the existence of multiple heme propionate conformations resulting, in large part, from the lack of H-bonded interactions with the substrate and/or H_4B, also due to the close proximity of the altered Glu-363 side chain.

Biochemical studies on NOS show that 7-NI is competitive against [^{3}H]H_4B (*21*, *25*), with an apparent inhibition constant (K_I measured for nNOS) of 120 nM (*23*, *24*) and given the similar inhibitory potency of 7-NI, in vitro, for all NOS isoforms (*39*), we would assume a comparable K_I value for eNOS as well. Furthermore, due to enhanced specificity of the brominated analogue over 7-NI (*22*), a similar or lower K_I would be expected for 7-NIBr. This would represent a 4-fold weaker affinity for 7-NI compared with the native cofactor [K_d = 30 nM for H_4B (*41*)]. Modifications to the indazole nucleus, such as the inclusion of the Br atom, could improve the affinity of the inhibitor for the H_4B site such that it approaches a value similar to the cofactor itself. Although there are no direct measurements of the ability of 7-NIBr to displace radiolabeled H_4B, seven additional nonbonded contacts made by the Br atom at the cofactor site would suggest an improved binding affinity. Given this scenario, it is difficult to predict whether 7-NIBr first displaces H_4B at the cofactor site or L-Arg at the substrate site. Should H_4B displacement by 7-NIBr occur first, lack of H-bonded interactions to the heme propionate would result in the weakening of the interaction between substrate and the propionate. Regardless of which site gets occupied first, the domino effect that follows 7-NIBr binding ensures a marked decrease in affinity at the second site for the native ligand. In essence, crystal structure analysis of the 7-NIBr-NOS interaction has allowed us to capture the exquisite cooperativity that exists between the substrate and cofactor binding sites. At the mechanistic level, these structural findings also reveal a concerted interplay between three nonprotein components (substrate, cofactor, and heme prosthetic group) to ensure a catalytically competent rotamer position for Glu-363.

eNOS − L-NNA Complex. 7-NI specifically competes with another nitro-containing NOS inhibitor (*24*, *41*), N^{ω}-nitro-L-Arg (L-NNA, Figure 1). Since L-NNA also contains a nitro group and is a potent inhibitor of NOS with K_d of approximately 25 nM (*23*), we asked if there are similarities in the modes of recognition between 7-NIBr and L-NNA, especially concerning the common nitro group in both inhibitors. To this end, we cocrystallized L-NNA with eNOS heme domain and solved and refined the structure to 1.80 Å resolution.

The binding mode of L-NNA (Figure 4B) at the substrate-binding site is similar to that of L-Arg insofar as the H-bonding and nonbonded contacts are concerned. The introduction of the nitro group, however, leads to new H-bonded interactions and nonbonded contacts with the inhibitor. First, backbone amide N atoms of two adjacent

residues, Gly-357 and Trp-358, respectively, act as H-bond donors to the two oxygen atoms of the nitro group. In the 7-NIBr bound structure, however, these amide nitrogens are in the vicinity of N2, C3, and Br atoms (Figure 4A). Second, thirteen new nonbonded contacts are established between L-NNA and the protein. All of these involve the nitro group of the inhibitor with Pro-336, Phe-355, Ser-356, Gly-357, and Trp-358 being the key residues making the contacts (Figure 4B). Again, these residues contact N1, N2, C3, and Br atoms in the 7-NIBr-complexed structure. Interestingly, one nonbonded contact, involving the carbonyl O of Trp-358 with an oxygen atom of the nitro group, is conserved in the interaction of both L-NNA and 7-NIBr with eNOS.

The substrate L-Arg has a K_d of 2.5 μM (*42*−*44*) while L-NNA exhibits a K_d of 25 nM (*23*), a roughly 4-fold greater affinity compared to 7-NI. The nitro group obviously plays a role in the improved potency of these compounds. As noted in the previous section, 7-NIBr derives at least part of its potency as a NOS inhibitor from electrostatic stabilization due to the electron-withdrawing properties of the nitro group as well as H-bonding. The effect of the nitro group is shared to some extent by L-NNA and 7-NI in that the nitro group provides new and favorable protein contacts. A major difference in 7-NI and L-NNA, however, is that L-NNA is a chiral molecule and the D-NNA enantiomer is neither a potent inhibitor of NOS in vitro (*12*) nor able to induce a pressor response in vivo (*45*). In fact, D-NNA is routinely used (*46*) as a negative control in experiments that also utilize the active enantiomer, L-NNA. The absolute need for chirality in L-NNA to confer specificity illustrates that the positioning of L-NNA similar to L-Arg at the substrate-binding site coaxes the nitro group into its binding pocket. The absence of a chiral restraint in 7-NI and 7-NIBr allows these inhibitors to choose a binding mode that would favor optimal stacking with the heme plane and avoid potential steric clashes. These structures of the inhibitor complexes reveal that the nitro group of L-NNA and 7-NIBr is recognized in two unique ways with L-NNA selecting the catalytically competent rotamer of Glu-363 and 7-NIBr opting for an altered rotamer of Glu-363, yet the nitro groups of both inhibitors form stabilizing protein contacts.

Inhibitor binding studies have revealed that H_4B binding to the cofactor site enhances L-NNA binding to the substrate site. The ability of H_4B to affect L-NNA binding varies between the three NOS isoforms (*32*), with nNOS showing marked improvement in L-NNA binding when cofactor is present (*44*). However, the binding of L-NNA in the active site as shown in Figure 4B is exactly the same in the pterin-free and -bound states. The only difference is that solvent occupies the pterin site in the pterin-free state. The observed dynamics of the Glu-363 side chain and the heme propionate suggest a plausible explanation of this phenomenon. If H_4B binding to the cofactor site stabilizes the propionate position for proper interaction with the primary amino group of L-NNA, then additional binding would be facilitated. As there are no additional sites for L-NNA binding on the heme domain, cooperativity between the pterin-site and L-Arg site as detailed by our structural findings can explain these observations.

Cofactor Binding Site of NOS Exhibits a High Level of Promiscuity. In an earlier study (*15*), we demonstrated the ability of the substrate, L-Arg, to bind to the H_4B binding site when a potent inhibitor S-ethylisothiourea (SEITU) was bound at the substrate site. Furthermore, it was not clear at that time why L-Arg cannot bind to the pterin site when it was also bound at the substrate-binding site. Upon observing that 7-NIBr independently occupies both substrate and cofactor binding sites at the same time, we questioned whether the inability of a compound, bound at the substrate site, to entertain H-bonded interactions with the heme propionate confers promiscuity to the H_4B site. To test this hypothesis, we chose two compounds that (1) had been shown to interact with NOS, and (2) retained some chemical features of both substrate and inhibitor.

The first compound, 7-nitroindazole-2-carboxamidine (NICA, Figure 1), has been reported in the literature (*30*) as an inhibitor of NOS. We cocrystallized this compound with pterin-complexed eNOS and solved the structure to assess the binding mode of the inhibitor. The crystal structure reveals that NICA binds to the pterin site (Figure 4C), but its binding mode is distinct from that of 7-NIBr. Specifically, the amidino function of the inhibitor establishes bidentate H-bonds with the same propionate that interacts with the pyramidone function when the pterin cofactor is bound. The interaction between the amindino group and heme propionate is very similar to the way the guanidinium group of L-Arg interacts with the heme propionate when L-Arg is bound in the H_4B site (*15*). The main difference is that L-Arg forms only one H-bond with the heme propionate. In addition, numerous nonbonded contacts are made between the indazole nucleus and the protein, similar to that seen with 7-NIBr. Interestingly, NICA is not bound at the substrate-site. Instead, the electron density could only be modeled as 7-NI (Figure 2). On the basis of the mode of 7-NIBr binding at the substrate site (Figure 4A), NICA would experience significant steric hindrance and explains why it is not bound at the L-Arg site. 7-NI is the precursor in the chemical synthesis of NICA, and residual amounts of this starting material are present even after purification. This is probably sufficient to bind at the substrate site. Regardless, the ability of the H_4B binding site to recognize yet another unique compound is established, and furthermore, it occurs only when the compound bound at the substrate site fails to make contact with the heme propionate.

The second compound we chose to test the promiscuity of H_4B site is 4-chlorophenyl hydroxyguanidine (CPHG, Figure 1). The elegant enzymological work of Mansuy and co-workers (*31*) has demonstrated that CPHG is a substrate of iNOS. Furthermore, the conversion of CPHG by NOS to the corresponding urea and NO has a strict requirement for H_4B analogous to the transformation of N^G-hydroxy-L-Arg (NOHA). More importantly, CPHG is incapable of engaging in H-bonded contacts with the heme propionate and, therefore, becomes a viable candidate to test the interplay between substrate site H-bonding patterns and cofactor site promiscuity. Again, we cocrystallized CPHG with pterin-free eNOS heme domain and solved and refined the structure to 1.95 Å resolution. Two molecules of CPHG are bound per heme domain subunit, one at the substrate-binding site and the other at the H_4B-binding site (Figure 4D). The electron density for both molecules of CPHG is clearly discernible (Figure 2). At the substrate site, CPHG participates in three H-bonded interactions exclusively involving the guanidinium group. Two of these include interactions from Glu-363 side chain

to NE and NH2 of CPHG and another between Trp-358 O and CPHG NH2. Although the hydroxyl group is within H-bonding distance (3.2 Å) to Gly-357 N, the geometry is unfavorable. The Cl atom of CPHG is involved in three nonbonded contacts. The interaction of the hydroxy-guanidine is analogous to that seen in the crystal structure of NOHA-complexed eNOS (*14*). When bound to the H_4B site, CPHG makes two H-bonded contacts involving both terminal guanidinium nitrogen and hydroxyl oxygen atoms, interacting with the backbone carbonyl O of Ala-448 and a heme propionate oxygen, respectively (Figure 4D). The −OH group is in a different conformation from that observed in the substrate binding site, also within H-bonding distance to the terminal guanidinium N of Arg-367. In addition, partial stacking between Trp-447 and the phenyl ring of CPHG, similar to that observed with 7-NIBr, is observed. The chlorine atom of CPHG, unlike Br of 7-NIBr, however, establishes all (13) of its nonbonded contacts with the second subunit. Over 60% of these contacts are made with the Gln-464 and Glu-465 pair. These results provide convincing evidence for the promiscuity of the H_4B binding site, particularly its ability to recognize structurally diverse ligands when one of the heme propionates is not engaged in H-bond interaction with an occupant of the substrate site in agreement with previous publications from our laboratories (*8*, *15*).

Implications for Drug Design. One implication of this work relates to the unusual way in which the inhibitor is bound. There are many instances in which a protein can distinguish between nearly identical inhibitors. For example, NOS recognizes the different arginine-based inhibitors by utilizing the same set of contacts that are made to L-Arg alongside new interactions made with the substituent. A case in point is the recognition of NNA described in the present study. Critical to this interaction is the H-bonding potential of Glu-363 side chain that participates in type I or type II interactions (*47*, *48*) depending on whether amidino (*49*), guanidino, or ureido (*50*) groups are present in the inhibitor. The 7-NIBr-bound eNOS structure provides a totally different scenario. First, it completely removes Glu-363 from engaging in direct H-bonded contact with the inhibitor. Second, by competing simultaneously for both the substrate and cofactor binding sites, 7-NIBr is able to occupy one site and subsequently alter the specificity of a second site. Structural analyses of the 7-NIBr-bound eNOS structure teaches us that designing an inhibitor, which avoids H-bonded contact with one of the heme propionates, can serve as a potential template for designing drugs with isoform specificity. This is because such compounds dramatically weaken the affinity of the cofactor site for H_4B and render it promiscuous. Therefore, one can take advantage of the small but significant differences at the substrate and cofactor binding sites toward designing bifunctional drugs with isoform selectivity.

The present work also has important implications for structure-based drug design. Usually, the target protein is treated as a binding surface template from which novel compounds with complementary shape and chemistry arise. In the conventional setting, a rigid geometry is assumed for the binding site, and this would not have predicted the binding of 7-NIBr to NOS. The ability of Glu-363 to adopt a different rotameric state, however, has been known from an earlier report (*51*), albeit involving catalytically inactive iNOS monomers. Although the previously identified conformer is different, cannot be assumed in the dimeric state, and is inconsequential to our description of a novel altered conformation, structural hints from Glu-363 side-chain dynamics provide a wealth of information. That Glu-363 adopts a new conformation in the 7-NIBr complex has provided a structural basis for introducing knowledge-based dynamics information into drug-design strategies for NOS. The present work also highlights the importance of dynamics, however small, in making a substantial contribution to the information content regarding how a target recognizes a ligand.

In summary, we have demonstrated that, although 7-NIBr targets the highly conserved substrate and cofactor-binding sites of NOS, its high specificity is garnered by adapting to a unique and altered protein conformation. The ability of 7-NIBr to exploit this characteristic element of its target provides a significant intellectual boost for the further development of therapeutically important isoform-specific NOS inhibitors.

ACKNOWLEDGMENT

C.S.R. is grateful to Pierre Nioche for a critical reading of the manuscript. C.S.R. was a Dorothy Penrose Stout fellow of the American Heart Association (Western States Affiliate) during the course of this work. We are grateful to the assistance provided by beamline staff at SSRL, CHESS, and ALS during data collection.

REFERENCES

1. Furchgott, R. F. (1999) *Angew. Chem., Int. Ed. Engl. 38*, 1870−1880.
2. Ignarro, L. J. (1999) *Angew. Chem., Int. Ed. Engl. 38*, 1882−1892.
3. Murad, F. (1999) *Angew. Chem., Int. Ed. Engl. 38*, 1857−1868.
4. Waldman, S. A., and Murad, F. (1987) *Pharmacol. Rev 39*, 163−196.
5. Denninger, J., and Marletta, M. (1999) *Biochim. Biophys. Acta 1411*, 334−350.
6. Lowenstein, C. J., Dinerman, J. L., and Snyder, S. (1994) *Ann. Intern. Med. 120*, 227−237.
7. Marletta, M. A. (1994) *Cell 78*, 927−930.
8. Raman, C. S., Martásek, P., and Masters, B. S. S. (2000) in *The Porphyrin Handbook* (Kadish, K. M., Smith, K. M., and Guilard, R., Eds.) Vol. 4, pp 293−339, Academic Press, San Diego.
9. Huang, Z., Huang, P. L., Panahian, N., Dalkara, T., Fishman, M. C., and Moskowitz, M. A. (1994) *Science 265*, 1883−1885.
10. Nathan, C. (1995) *Cell 82*, 873−876.
11. Babu, B. R., and Griffith, O. W. (1998) *Curr. Opin. Chem. Biol. 2*, 491−500.
12. Southan, G. J., and Szabo, C. (1996) *Biochem. Pharmacol. 51*, 383−394.
13. Crane, B. R., Arvai, A. S., Ghosh, D. K., Wu, C., Getzoff, E. D., Stuehr, D. J., and Tainer, J. A. (1998) *Science 279*, 2121−2126.
14. Fischmann, T. O., Hruza, A., Niu, X. D., Fossetta, J. D., Lunn, C. A., Dolphin, E., Prongay, A. J., Reichert, P., Lundell, D. J., Narula, S. K., and Patricia, C. W. (1999) *Nat. Struct. Biol. 6*, 233−242.
15. Raman, C. S., Li, H., Martásek, P., Král, V., Masters, B. S., and Poulos, T. L. (1998) *Cell 95*, 939−950.
16. Hawkey, C. J. (1999) *Lancet 353*, 307−314.
17. Kalgutkar, A. S., Crews, B. C., Rowlinson, S. W., Garner, C., Seibert, K., and Marnett, L. J. (1998) *Science 280*, 1268−1270.

18. Kurumbail, R. G., Stevens, A. M., Gierse, J. K., McDonald, J. J., Gildehaus, D., Miyashiro, J. M., Penning, T. D., Seibert, K., Isakson, P. C., and Stallings, W. C. (1996) *Nature 384*, 644−648.
19. Babbedge, R. C., Bland-Ward, P. A., Hart, S. L., and Moore, P. K. (1993) *Br. J. Pharmacol. 110*, 225−228.
20. Moore, P. K., Wallace, P., Gaffen, Z., Hart, S. L., and Babbedge, R. C. (1993) *Br. J. Pharmacol. 110*, 219−224.
21. Wolff, D. J., Lubeskie, A., and Umansky, S. (1994) *Arch. Biochem. Biophys. 314*, 360−366.
22. Bland-Ward, P. A., and Moore, P. K. (1995) *Life Sci. 57*, 131−135.
23. Alderton, W. K., Boyhan, A., and Lowe, P. N. (1998) *Biochem. J. 332*, 195−201.
24. Mayer, B., Klatt, P., Werner, E. R., and Schmidt, K. (1994) *Neuropharmacol. 33*, 1253−1259.
25. Wolff, D. J., and Gribin, B. J. (1994) *Arch. Biochem. Biophys. 311*, 300−306.
26. Handy, R. L. C., and Moore, P. K. (1998) *Trends Pharm. Sci. 19*, 350.
27. Nanri, K., Montecot, C., Springhetti, V., Seylaz, J., and Pinard, E. (1998) *Stroke 29*, 1248−1254.
28. Przedborski, S., Jackson-Lewis, V., Yokoyama, R., Shibata, T., Dawson, V. L., and Dawson, T. M. (1996) *Proc. Natl. Acad. Sci. U.S.A. 93*, 4565−4571.
29. Zhang, Y., Dawson, V. L., and Dawson, T. M. (2000) *Neurobiol. Dis. 7*, 240−250.
30. Southan, G. J., Gauld, D., Lubeskie, A., Zingarelli, B., Cuzzocrea, S., Salzman, A. L., Szabo, C., and Wolff, D. J. (1997) *Biochem. Pharmacol. 54*, 409−417.
31. Renodon-Corniere, A., Boucher, J. L., Dijols, S., Stuehr, D. J., and Mansuy, D. (1999) *Biochemistry 38*, 4663−4668.
32. Martásek, P., Liu, Q., Liu, J., Roman, L. J., Gross, S. S., Sessa, W. C., and Masters, B. S. (1996) *Biochem. Biophys. Res. Commun. 219*, 359−365.
33. Otwinowski, Z., and Minor, W. (1997) *Methods Enzymol. 276*, 307−326.
34. Brunger, A. T., Adams, P. D., Clore, G. M., DeLano, W. L., Gros, P., Grosse-Kunstleve, R. W., Jiang, J.-S., Kuszewski, J., Nilges, M., Pannu, N. S., Read, R. J., Rice, L. M., Simonson, T., and Warren, G. L. (1998) *Acta Crystallogr., Sect. D 54*, 905−921.
35. Jones, T. A. (1985) *Methods Enzymol. 115*, 157−171.
36. Sheldrick, G. M., and Schneider, T. R. (1997) *Methods Enzymol. 277*, 319−343.
37. Chen, P. F., Tsai, A. L., Berka, V., and Wu, K. K. (1997) *J. Biol. Chem. 272*, 6114−6118.
38. Gachhui, R., Ghosh, D. K., Wu, C., Parkinson, J., Crane, B. R., and Stuehr, D. J. (1997) *Biochemistry 36*, 5097−5103.
39. Moore, P. K., and Bland-Ward, P. A. (1996) *Methods Enzymol. 268*, 393−398.
40. Honig, B., and Nicholls, A. (1995) *Science 268*, 1144−1149.
41. Gross, S. S., Jones, C. L., Hattori, Y., and Raman, C. S. (2000) in *Nitric Oxide* (Ignarro, L. J., Ed.) Academic Press, New York.
42. Berka, V., Chen, P.-F., and Tsai, A.-L. *J. Biol. Chem. 271*, 33293−33300.
43. Boyhan, A., Smith, D., Charles, I. G., Saqi, M., and Lowe, P. N. (1997) *Biochem. J. 323*, 131−139.
44. Roman, L. J., Sheta, E. A., Martásek, P., Gross, S. S., Liu, Q., and Masters, B. S. (1995) *Proc. Natl. Acad. Sci. U.S.A. 92*, 8428−8432.
45. Wang, Y.-X., Cheng, X., and Pang, C. C. (1999) *Eur. J. Pharmacol. 366*, 175−179.
46. Islas-Cadena, M., Aguirre-Banuelos, P., and Granados-Soto, V. (1999) *J. Pharmacol. Toxicol. Methods 42*, 87−92.
47. Ippolito, J. A., Alexander, R. A., and Christianson, D. W. (1990) *J. Mol. Biol. 215*, 457−471.
48. Singh, J., Thornton, J. M., Snarey, M., and Campbell, S. F. (1987) *FEBS Lett. 224*, 161−171.
49. Li, H., Raman, C. S., Martásek, P., Masters, B. S. S., and Poulos, T. L. (2001) *Biochemistry 40*, 5399−5406.
50. Li, H., Raman, C. S., Martásek, P., Král, V., Masters, B. S. S., and Poulos, T. L. (2000) *J. Inorg. Biochem. 81*, 133−139.
51. Crane, B. R., Arvai, A. S., Gachhui, R., Wu, C., Ghosh, D. K., Getzoff, E. D., Stuehr, D. J., and Tainer, J. A. (1997) *Science 278*, 425−431.

BI010957U